

Modeling for control of a three degrees-of-freedom Magnetic Levitation System

Rafael Becerril-Arreola

Manfredi Maggiore

Dept. of Electrical and Computer Eng. Dept. of Electrical and Computer Eng.

University of Toronto

University of Toronto

10 King's College Road

10 King's College Road

Toronto ON M5S 3G4

Toronto ON M5S 3G4

Systems Control Group Report No. 0204

March 17, 2003

Abstract

This paper presents the derivation of the model for a high-precision positioning system using magnetic levitation, which is achieved by an arrangement of Permanent Magnet Linear Synchronous Motors. LQR set-point stabilization is performed as an introduction to the more advanced nonlinear control design presented in [9].

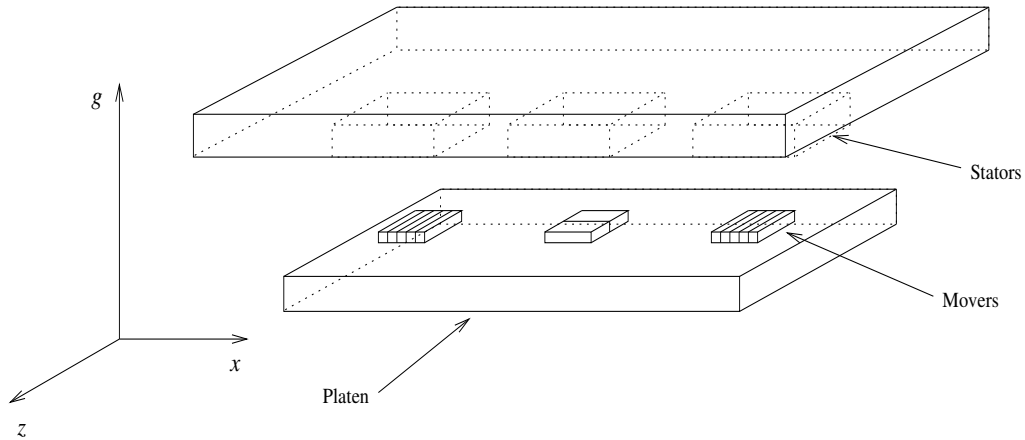


Figure 1: Configuration with three LSMs to achieve three degrees of freedom

1 Introduction

We consider the problem of preventing the production of free particles on high precision positioning systems, like those used in photolithography. To this end, replacement of bearings with magnetic levitation is proposed. This yields a similar solution to the one shown in [6]¹. However, the alternative presented here involves the use of already existing technologies while spawning an attractive control design problem.

Almost invariably, linear motors are used under the constraint of a constant airgap enforced by means of bearings. Magnetic and dynamic models of linear motors have been developed within this context. Nevertheless, in order to achieve levitation, airgap control must be performed beside positioning control. In this document, a detailed analytical model considering a variable airgap is introduced. As shown later, this model is highly nonlinear. For this purpose, the results developed for a fixed airgap in [1] are revisited in order to take into account a variable airgap. Afterwards, the model is enhanced by including the effect of the stator slots on the field distribution, this is accomplished by building on top of the fundamentals given in [4]. For the sake of illustration, we briefly present the results of a linear control design. A rigorous nonlinear control design approach based on this model can be found in [9].

2 Problem statement

Consider the setup shown in Figure 1, where three PMLSMs (Permanent Magnet Linear Synchronous Motors) drive a floating platen. The system employs three identical motors equally spaced along a straight line and perpendicularly oriented with respect to each other. The windings of motors 1 and 3 (those at the ends of the structure) are connected in parallel whereas motor 2 is fed independently. In order to allow long travel, the movers of the motors are significantly smaller than their stators..

In each of the three motors, the permanent magnets are placed on the surface of a flat structure of ferromagnetic material (the mover), as shown in Figure 2. Every stator made of longitudinal laminations and transversally slotted in order to house three-phase windings, as shown in Figure 2. In addition to the previous specifications, the design takes into account the following constraints.

Assumption 1. The motors are far enough from each other so that their fields do not interfere with each other.

In addition, the model developed in this chapter is valid provided that the movement of the platen never drives the permanent magnets outside of the areas covered by the stators' magnetic fields. Moreover, if the movers never get too close to the borders of such regions, modelling can assume uniform effects at the ends of the movers. Making sure that such conditions are always met is a control design objective.

Remark 1. Since the forces are periodically exerted all over the surfaces of the movers, the resultant torque sums zero. Therefore, rotation is prevented and translational dynamics yield a complete model of the system.

3 Modeling

In order to obtain a model describing each of the motors, a detailed electromagnetic analysis is required. The components of the electromagnetic forces acting on the mover of the motor, i.e. the thrust and the normal force, can be obtained by independently computing the fields produced by the permanent magnets and the stator windings. The obtained analytical expressions for the resultant magnetic field are then used to compute the forces exerted on the surfaces of the permanent magnets.

For most of the following development, we use the results in [1] and [4] by, to some extent, merging them. Some

¹Actually, [6] presents the only one experimental test bed for this problem with technology similar to the one we use.

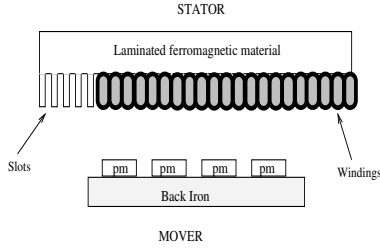


Figure 2: Configuration of a single PMLSM

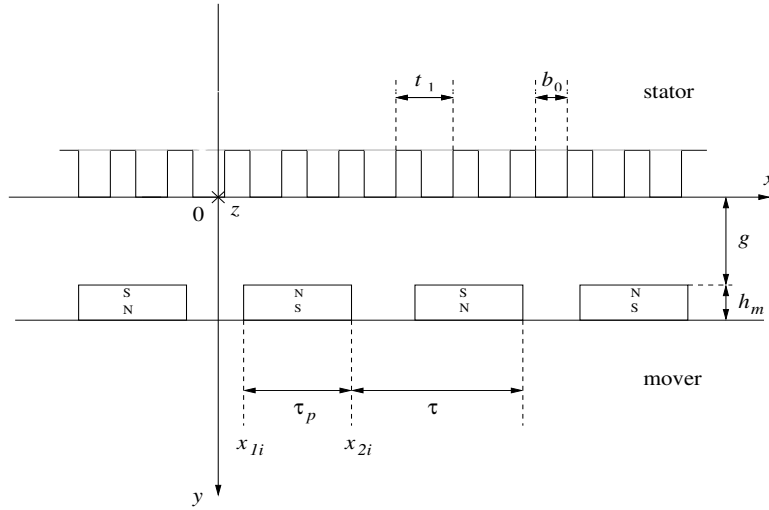


Figure 3: Frame-set considered in the analysis

details are included *primarily* for convenience of the reader, but also to emphasize the differences between [1] and this development.

Hereafter, the magnetic field density produced by the permanent magnets B_{pm} will be found by first computing the corresponding magnetic field intensity \vec{H}_{pm} . This is achieved by relying of the images method, which allows us to easily find the magnetic potential of the permanent magnets, Ψ_{pm} .

The frame-set under which all quantities are measured is depicted in Figure 3. By establishing an analogy, some magnetic problems can be solved by applying the methods developed for electric fields. We use this analogy in order to find the magnetic field density produced by the permanent magnets on the mover. Considering a permanent magnet with parallelepipedal shape and a uniform distribution of Ψ_{pm} , by virtue of the mentioned analogy and from standard

electrostatic analysis, the magnetic potential at a point $P = (x, y, z)$ in the vicinity of the magnet is given by

$$\Psi_{pm}(x, y, z) = \frac{1}{4\pi} \left(\int_{S_1} \frac{\sigma_m dS_1}{r_1} - \int_{S_2} \frac{\sigma_m dS_2}{r_2} \right). \quad (1)$$

Where σ_m is the magnetic charge, S_1 and S_2 are the two surfaces perpendicular to the magnetization vector of the PM, and r_1 and r_2 are the lengths of the vectors from S_1 and S_2 to the point P , respectively. The magnetic field intensity is then found by noting that $\vec{H}_{pm} = -\nabla\Psi_{pm}$

$$\vec{H}_{pm} = \frac{1}{4\pi} \left(\int_{S_1} \frac{\sigma_m \vec{r}_1 dS_1}{r_1^3} - \int_{S_2} \frac{\sigma_m \vec{r}_2 dS_2}{r_2^3} \right). \quad (2)$$

Let h_m be the height of the magnets and g be the airgap between the magnets and the stator (see Figure 3).

By knowing the charge in the interior of the magnet and the potential on its boundary, it is possible to determine the potential on the surrounding space. This is accomplished by finding the Green function which satisfies the Poisson's equation for the magnetic potential. However, due to the high symmetry of the problem, the simpler method of images can be applied (see, e.g, [7]).

The method of images is commonly applied to find the electric potential due to a charge in presence of an equipotential surface, such as a conductor. Its main idea is to replace the equipotential region by a charge which is the mirror of the actual charge with respect to such region. In our case, and due to the ferromagnetic material, the surfaces of the mover and the stator are equipotential surfaces. When the charge is located between two equipotential parallel surfaces, an infinite set of images is obtained. For the i th pole, the charge of its k th image is $\sigma_m(i, k) = (-1)^{k+i} \sigma_m$. Let h_k be the position of the k th image and σ_m its charge. Let $g_e = gK_c$ be the effective airgap due to the effect of the slots in the stator and K_c the Carter's coefficient, which is a parameter containing information relative to the topology of the motor. K_c is given by

$$K_c = \frac{t_1}{t_1 - g\gamma_1}, \quad \gamma_1 = \frac{4}{\pi} \left[\frac{b_0}{2g} \arctan\left(\frac{b_0}{2g}\right) - \ln \sqrt{1 + \left(\frac{b_0}{2g}\right)^2} \right], \quad (3)$$

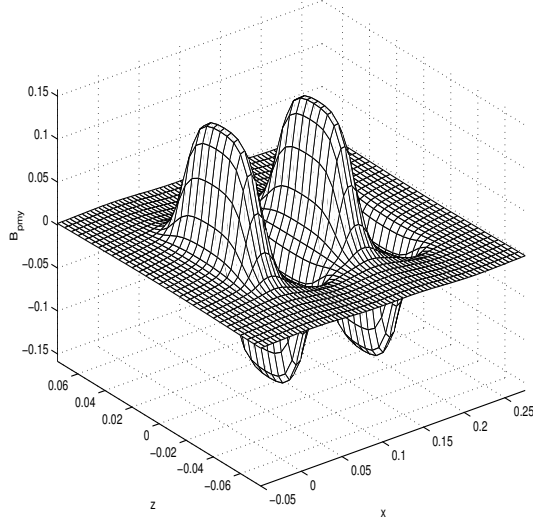


Figure 4: Magnetic field density on the stator's surface

being t_1 the slot pitch and b_0 the slot aperture, as shown in Figure 3. The positions of the images, h_k are

$$h_k = \begin{cases} (k+1)h_m + kg_e & \text{when } k \text{ is odd} \\ kh_m + (k+1)g_e & \text{when } k \text{ is even.} \end{cases} \quad (4)$$

Let L_A be the depth of the poles along the z direction, τ be the permanent magnets pole pitch (i.e, the distance between poles centers), p_m be the number of permanent magnets and τ_p be the permanent magnets pole arc (see Figure 3). We are ready to calculate the magnetic potential due to the permanent magnets at any given point $P = (x_0, y_0, z_0)$ in the airgap. The y component of H_{pm} is given by

$$H_{pmy}(x_0, y_0, z_0, g) = \frac{\sigma_m}{4\pi} \sum_{i=1}^{p_m} \sum_{k=-\infty}^{\infty} (-1)^{k+i} \left[\arctan \frac{(x_0 - x)(z_0 - z)}{(y_0 - h_k)D_k} \right] \Bigg|_{x=x_{2i}}^{x=x_{1i}} \Bigg|_{z=-L_A/2}^{z=L_A/2}, \quad (5)$$

where

$$D_k = \sqrt{(x_0 - x)^2 + (y_0 - h_k)^2 + (z_0 - z)^2}, \quad x_{1i} = \left(i - \frac{1+\alpha}{2}\right)\tau, \quad x_{2i} = \left(i - \frac{1-\alpha}{2}\right)\tau, \quad \alpha = \frac{\tau_p}{\tau}.$$

Evaluating (5) on a grid of values of (x_0, z_0) with $y_0 = 0$ and $g = 0.01$ m, and multiplying by the free space permeability,

μ_0 , the plot of $B_{pmy}(x_0, y_0 = 0, z_0, g = 0.01)$ in Figure 4 is obtained.

Since a closed form for (5) is impossible to obtain, we fix the value of the airgap, $g = g_0$, and proceed to numerically average the field intensity. This is achieved by averaging along the z axis after substitution of $g = g_0$, thus obtaining a function $H_{pmyav}(x_0, y_0)$. Next, in order to find the field intensity on the surface of the stator, we let $y_0 = 0$ thus obtaining

$$H_{pmyav}(x_0, 0) = \frac{2}{L_A} \int_0^{L_A/2} H_{pmy}(x_0, y_0 = 0, z_0, g = g_0) dz_0. \quad (6)$$

Numerical results revealed that (6) describes an almost sinusoidal function. Hence, H_{pmyav} can be approximated by calculating its Fourier series first harmonic without considerable loss of accuracy. The coefficient of the first harmonic is given by

$$H_{pmy1} = \frac{4}{\tau} \int_{n\tau}^{n\tau+\tau/2} H_{pmyav}(x_0, 0) \sin\left(\frac{\pi}{\tau}x_0\right) dx_0, \quad (7)$$

with $n = \frac{p_m}{2}$, where p_m is the number of poles. By noting that, in the airgap, $\vec{B} = \mu_0\vec{H}$, we conclude that the y component of the flux density due to the permanent magnets can be approximated by

$$B_{pmy} \approx B_{pmy1} = \mu_0 H_{pmy1} \sin\left(\frac{\pi}{\tau}x\right). \quad (8)$$

Figure 5 shows the field intensity distribution along x and its fundamental harmonic. Note that the sinusoidal approximation is rather accurate in the range of interest.

Remark 2. As mentioned above, (8) holds for a fixed value of the airgap g_0 . Since we need to consider a variable airgap, one has that B_{pmy} is also a function of g . We therefore numerically calculate the coefficient $\mu_0 H_{pmy1}$ for several different values of g in the range of interest and approximate the unknown function $B_{pmy1}(g)$ by polynomial interpolation, as shown in Figure 6.

Once the magnetic field density pertaining to the permanent magnets is known, we need to calculate the one produced by the stator. Here, we again closely follow the development in [1], where the magnetomotive force (mmf) of the traveling magnetic field is found in order to calculate Ψ_m , which will be used to obtain B . Let d denote the

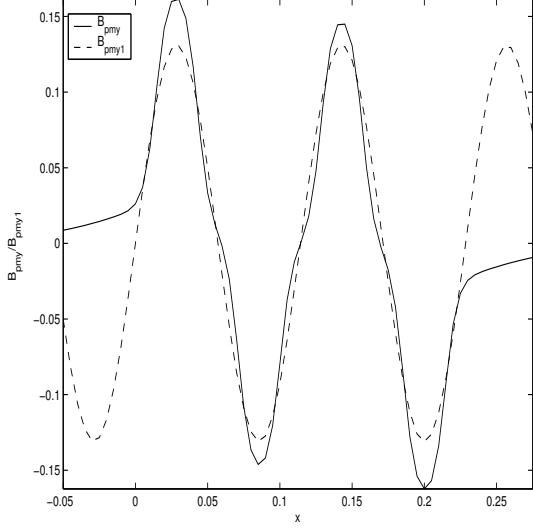


Figure 5: Magnetic field density along x axis

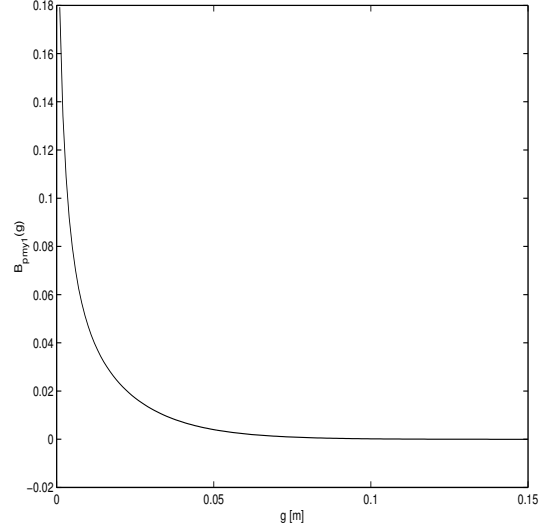


Figure 6: Magnetic field density as function of g

relative position of the mover with respect to the stator. The coefficient of the first harmonic of the mmf generated by the traveling magnetic field of the stator of a three-phase LSM is

$$\mathcal{F}_{s1} = \frac{6\sqrt{2}WI_a k_{w1}}{\pi K_c p} \sin \left[(x-d) \frac{\pi}{\tau} \right], \quad (9)$$

where W is the number of turns of wire on each phase, I_a is the armature current, p is the number of poles, w_c is the coil pitch, and k_{wm} is the winding factor. Once \mathcal{F}_{s1} has been found, it can be used to compute the first harmonic of the magnetic potential, which is given by

$$\Psi_{s1} = \mathcal{F}_{s1} \left[\cosh \left(\frac{\pi}{\tau} y \right) - \frac{\cosh \left[\frac{\pi}{\tau} (h_m + g) \right]}{\sinh \left[\frac{\pi}{\tau} (h_m + g) \right]} \sinh \left(\frac{\pi}{\tau} y \right) \right] \sin \left(\frac{\pi}{\tau} x \right). \quad (10)$$

Then, the components of the first harmonic of the magnetic field density produced by the stator are

$$\begin{aligned} B_{s1x} &= -\mu_0 H_{s1x} = -\mu_0 \frac{\partial \Psi_{s1}}{\partial x} = -\mu_0 \frac{\pi}{\tau} \mathcal{F}_{s1} \frac{\sinh \left[\frac{\pi}{\tau} (h_m + g - y) \right]}{\sinh \left[\frac{\pi}{\tau} (h_m + g) \right]} \cos \left(\frac{\pi}{\tau} x \right) \\ B_{s1y} &= -\mu_0 H_{s1y} = -\mu_0 \frac{\partial \Psi_{s1}}{\partial y} = -\mu_0 \frac{\pi}{\tau} \mathcal{F}_{s1} \frac{\cosh \left[\frac{\pi}{\tau} (h_m + g - y) \right]}{\sinh \left[\frac{\pi}{\tau} (h_m + g) \right]} \sin \left(\frac{\pi}{\tau} x \right). \end{aligned} \quad (11)$$

The difference between the reluctances of the slots and the teeth of the stator (see Figure 7) produces spatial modulation on the distribution of the field. This phenomenon, referred to as the *slots effect*, is accounted for by

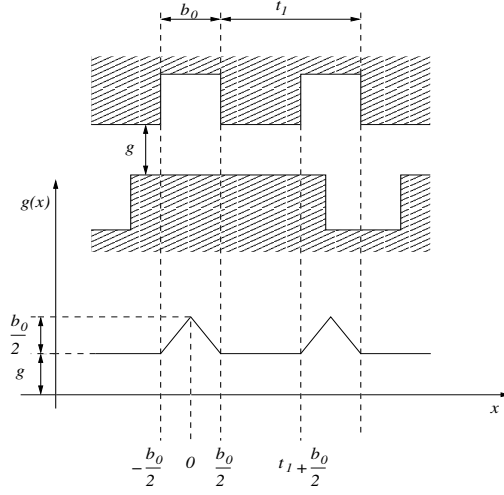


Figure 7: Relationship between the actual slots and the function $g(x)$

multiplying the field density, B , by the relative permeance $\tilde{\lambda}$ on the forces expressions.

Remark 3. In order to obtain the expression for the relative permeance, we adapt the concept presented in [4] for permanent magnet DC motors and develop the linear variable airgap version.

As stated in [4], the relative permeance $\tilde{\lambda}$ is given by

$$\tilde{\lambda} = \frac{g + \frac{h_m}{\mu_{rec}}}{g(x) + \frac{h_m}{\mu_{rec}}}, \quad (12)$$

being g the original gap (considered as a constant for this part of the analysis) and $g(x)$ the shortest distance that the flux lines have to travel through the slots before reaching the teeth when leaving the magnets from a point x (see Figure 7). In order to find an analytical expression for this function, we need the following assumption.

Assumption 2. The magnetic flux lines travel vertically through the airgap and horizontally in the slots. In other words, we assume that the pitch of the slot is greater than its depth. Elementary calculations lead to the following expression for $g(x)$

$$g(x) = \begin{cases} g + kt_1 + \frac{b_0}{2} - |x| & kt_1 - \frac{b_0}{2} \leq x \leq kt_1 + \frac{b_0}{2} \\ g & kt_1 + \frac{b_0}{2} \leq x \leq (k+1)t_1 - \frac{b_0}{2}, \end{cases} \quad (13)$$

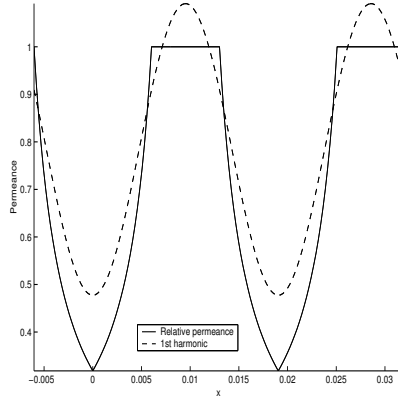


Figure 8: Relative permeance and its first harmonic

where k is the index of each slot, b_0 the width of the slot and w_c the coil pitch. Since (13) is a piecewise continuous function, we obtain its Fourier series representation. Figure 8 shows a plot of the relative permeance, and its first harmonic approximation (dashed line). To simplify calculations, we define the function $h(x)$ as follows

$$h(x) = \frac{1}{g(x) + \frac{h_m}{\mu_{rec}}}, \quad (14)$$

where μ_{rec} is the relative recoil permeability of the permanent magnets. Moreover, since we are dealing with a periodic function that will be approximated by its Fourier series, without loss of generality, calculations can be performed for $k = 1$. Hence, $h(x)$ is reduced to

$$h(x) = \begin{cases} \frac{1}{g + \frac{b_0}{2} + \frac{h_m}{\mu_{rec}}} + \frac{|x|}{(g + \frac{h_m}{\mu_{rec}})(g + \frac{b_0}{2} + \frac{h_m}{\mu_{rec}})} & -\frac{b_0}{2} \leq x \leq \frac{b_0}{2} \\ \frac{1}{g + \frac{h_m}{\mu_{rec}}} & \frac{b_0}{2} \leq x \leq t_1 - \frac{b_0}{2}. \end{cases} \quad (15)$$

In terms of $h(x)$, the relative permeance is given by

$$\tilde{\lambda} = \left(g + \frac{h_m}{\mu_{rec}} \right) h(x). \quad (16)$$

After few calculations, the Fourier series of $h(x)$ is obtained as

$$\begin{aligned}
h(x) &= a_0 + \sum_{n=1}^{\infty} a_n \cos\left(\frac{2\pi n}{t_1}x\right) \\
&= \frac{1}{g + \frac{h_m}{\mu_{rec}}} - \frac{b_0^2}{4t_1\left(g + \frac{h_m}{\mu_{rec}}\right)\left(g + \frac{b_0}{2} + \frac{h_m}{\mu_{rec}}\right)} \\
&\quad + \frac{t_1}{\pi^2\left(g + \frac{h_m}{\mu_{rec}}\right)\left(g + \frac{b_0}{2} + \frac{h_m}{\mu_{rec}}\right)} \sum_{n=1}^{\infty} \left[\cos\left(\frac{n\pi b_0}{t_1}\right) - 1\right] \cos\left(\frac{2\pi n}{t_1}x\right).
\end{aligned} \tag{17}$$

Thus, the relative permeance is given by

$$\begin{aligned}
\tilde{\lambda} &= 1 - \frac{b_0^2}{4t_1\left(g + \frac{b_0}{2} + \frac{h_m}{\mu_{rec}}\right)} \\
&\quad + \frac{t_1}{\pi^2\left(g + \frac{b_0}{2} + \frac{h_m}{\mu_{rec}}\right)} \sum_{n=1}^{\infty} \left[\cos\left(\frac{n\pi b_0}{t_1}\right) - 1\right] \cos\left(\frac{2\pi n}{t_1}x\right).
\end{aligned} \tag{18}$$

Remark 4. Now, we use (18) to find expressions for the thrust and the normal force, according to the method described in [1] but, unlike [1], allowing for a variable airgap.

Regarding the stator surface as a surface S of charged particles, we can find the motors thrust by considering the x component of the traveling magnetic field, given in (11), which is affected by the relative permeance given in (18).

The thrust magnitude is given by

$$F_x \approx p_m L_A \sigma_m \int_{-\frac{\tau_p}{2}}^{\frac{\tau_p}{2}} \tilde{\lambda} B_{s1x} dx \tag{19}$$

$$\approx \frac{\rho}{K_c \sinh\left[\frac{\pi}{\tau}(g + h_m)\right]} \left[\eta - \frac{\zeta}{g + \frac{b_0}{2} + \frac{h_m}{\mu_{rec}}} \right] I_a \sin\left(\frac{\pi}{\tau}d\right), \tag{20}$$

where

$$\rho = \frac{12\sqrt{2}k_w1 p_m L_A \sigma_m \mu_0 \sinh\left(\frac{\pi}{\tau}h_m\right)}{\pi p} \tag{21}$$

$$\zeta = \frac{b_0^2}{4t_1} \eta + \bar{\Lambda} \tag{22}$$

$$\eta = \sin\left(\frac{\pi\tau p}{2\tau}\right) \tag{23}$$

$$\bar{\Lambda} = \frac{t_1}{2\pi\tau} \sum_{n=1}^{\infty} \left[\cos\left(\frac{n\pi b_0}{t_1}\right) - 1\right] \Lambda_n \tag{24}$$

$$\Lambda_n = \left\{ \frac{\sin \left[\left(\frac{2n\pi}{t_1} + \frac{\pi}{\tau} \right) \frac{\tau_p}{2} \right]}{\frac{2n\pi}{t_1} + \frac{\pi}{\tau}} + \frac{\sin \left[\left(\frac{\pi}{\tau} - \frac{2n\pi}{t_1} \right) \frac{\tau_p}{2} \right]}{\frac{\pi}{\tau} - \frac{2n\pi}{t_1}} \right\}. \quad (25)$$

The normal force can be found from the definition of the Maxwell stress tensor (see [8]) and from the resultant magnetic field on the airgap, which is given by

$$B_{gy}^2 = B_{s1y}^2 + B_{pmy}^2 + 2B_{s1y}B_{pmy} \cos \left(\frac{\pi}{\tau} d \right). \quad (26)$$

Recall that the density fields on the right hand side of (26) is a function of g . In order to ease the calculations, only the fundamental component $\tilde{\lambda}_0$ and the first harmonic of the permeance $\tilde{\lambda}_1$ are considered. Thus the normal force is

$$\begin{aligned} F_y &\approx \frac{\rho_m L_A}{2\mu_0} \int_0^\tau \left[\tilde{\lambda}_1 B_g \sin \left(\frac{\pi}{\tau} x \right) \right]^2 dx \\ &\approx \Upsilon \left\{ \frac{\varphi^2 I_a^2}{K_c^2} \coth^2 \left[\frac{\pi}{\tau} (g + h_m) \right] + B_{pmy}^2(g) + \frac{2\varphi I_a B_{pmy}(g)}{K_c} \coth \left[\frac{\pi}{\tau} (g + h_m) \right] \cos \left(\frac{\pi}{\tau} d \right) \right\} \Gamma(g) \end{aligned} \quad (27)$$

where

$$\Upsilon = \frac{\rho_m L_A}{2\mu_0} \quad (28)$$

$$\varphi = \frac{6\sqrt{2}k_w \mu_0}{p\tau} \quad (29)$$

$$\Gamma(g) = \frac{\tau}{2} - \frac{\vartheta}{g + \frac{b_0}{2} + \frac{h_m}{\mu_{rec}}} + \frac{\varsigma}{2(g + \frac{b_0}{2} + \frac{h_m}{\mu_{rec}})^2} \quad (30)$$

$$\vartheta = \frac{\tau b_0^2}{4t_1} + \frac{\xi - \beta}{\pi^2} \left[\cos \left(\frac{\pi b_0}{t_1} \right) - 1 \right] t_1 \quad (31)$$

$$\varsigma = \frac{\tau b_0^4}{16t_1^2} - \frac{b_0^2(\xi - \beta)}{2\pi^2} \left[\cos \left(\frac{\pi b_0}{t_1} \right) - 1 \right] + \frac{2\varpi t_1^2}{\pi^4} \left[\cos \left(\frac{\pi b_0}{t_1} \right) - 1 \right] \quad (32)$$

$$\xi = \frac{t_1}{2\pi} \sin \left(\frac{2\pi\tau}{t_1} \right) \quad (33)$$

$$\beta = \frac{\sin \left[\frac{2\pi(\tau+t_1)}{t_1} \right] \tau t_1}{4\pi(\tau+t_1)} + \frac{\sin \left[\frac{2\pi(\tau-t_1)}{t_1} \right] \tau t_1}{4\pi(\tau-t_1)} \quad (34)$$

$$\varpi = \frac{\tau}{4} + \frac{t_1}{16\pi} \sin \left(\frac{4\pi\tau}{t_1} \right) - \frac{1}{4} \left\{ \frac{\sin \left[\frac{2\pi(2\tau+t_1)}{t_1} \right] \tau t_1}{2\pi(2\tau+t_1)} + \frac{\sin \left[\frac{2\pi(2\tau-t_1)}{t_1} \right] \tau t_1}{2\pi(2\tau-t_1)} \right\}. \quad (35)$$

$\Gamma(g)$ is the term that accounts for the effect of the slots. If that effect is to be neglected, $\Gamma(g) = \Gamma = \frac{\tau}{2}$.

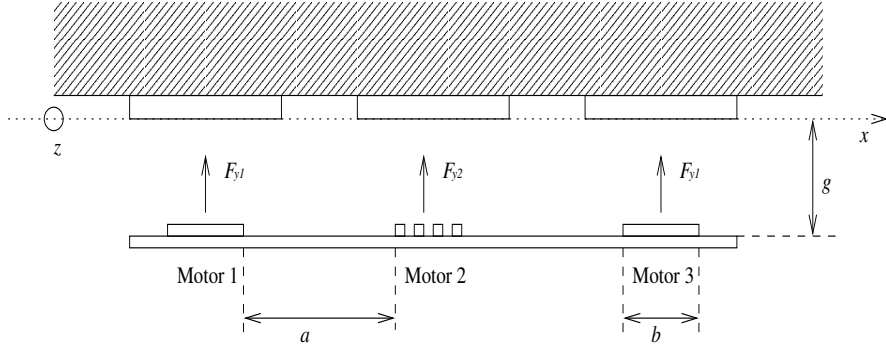


Figure 9: Forces in the three LSMs configuration

In order to derive the dynamic model of the magnetic levitation system shown in Figure 1, let M_p be the mass of the platen, G the gravity constant, and i_d, i_q be the direct and quadrature currents which are regarded as the control inputs. For $\mathbf{x} = [g, \dot{g}, x, \dot{x}, z, \dot{z}]^T$ and the forces defined as in Figure 9, Newton laws yield the following equations

$$\begin{aligned}
 M_p \ddot{g} &= M_p G - 2F_{y1}(g, z) - F_{y2}(g, x) \\
 M_p \ddot{x} &= F_x(g, x) \\
 M_p \ddot{z} &= 2F_z(g, z)
 \end{aligned} \tag{36}$$

where x and z are the displacements in the x and z directions respectively, $F_{y1} = F_{y1}(x_1, x_5, i_{d1}, i_{q1})$ and $F_z = F_z(x_1, x_5, i_{d1}, i_{q1})$ are the forces generated by motor 1 and 3, and $F_{y2} = F_{y2}(x_1, x_3, i_{d2}, i_{q2})$ and $F_x = F_x(x_1, x_3, i_{d2}, i_{q2})$ are the forces produced by motor 2. F_x, F_{y1}, F_{y2} and F_z are given by expressions (20) and (27). The dynamics become

$$\dot{\mathbf{x}} = \begin{bmatrix} x_2 \\ G - \frac{2F_{y1}}{M_p} - \frac{F_{y2}}{M_p} \\ x_4 \\ \frac{F_x}{M_p} \\ x_6 \\ 2\frac{F_z}{M_p} \end{bmatrix}. \tag{37}$$

Expression (37) can be expanded by substituting the full expressions of the forces, yielding

$$\begin{aligned}
\dot{x}_1 &= x_2 \\
\dot{x}_2 &= G - \frac{\Upsilon\Gamma(x_1)}{M_p} \frac{\varphi^2}{K_c^2(x_1)} \coth^2 \left[\frac{\pi}{\tau}(x_1 + h_m) \right] [2(i_{d1}^2 + i_{q1}^2) + i_{d2}^2 + i_{q2}^2] \\
&\quad - \frac{\Upsilon\Gamma(x_1)}{M_p} \left\{ 3B_{pmy}^2(x_1) + \frac{2\varphi B_{pmy}(x_1)}{K_c(x_1)} \coth \left[\frac{\pi}{\tau}(x_1 + h_m) \right] [2i_{d1} + i_{d2}] \right\} \\
\dot{x}_3 &= x_4 \\
\dot{x}_4 &= \frac{\rho}{M_p K_c(x_1) \sinh \left[\frac{\pi}{\tau}(x_1 + h_m) \right]} \left[\eta - \frac{\zeta}{x_1 + \frac{b_0}{2} + \frac{h_m}{\mu_{rec}}} \right] i_{q2} \\
\dot{x}_5 &= x_6 \\
\dot{x}_6 &= \frac{2\rho}{M_p K_c(x_1) \sinh \left[\frac{\pi}{\tau}(x_1 + h_m) \right]} \left[\eta - \frac{\zeta}{x_1 + \frac{b_0}{2} + \frac{h_m}{\mu_{rec}}} \right] i_{q1}.
\end{aligned} \tag{38}$$

Introducing the change in notation given by

$$\begin{aligned}
\beth &= \frac{\Upsilon}{M_p} \varphi^2 & \nu &= \frac{2\varphi\Upsilon}{M_p} \\
\chi &= \frac{3\Upsilon}{M_p} & \beth &= \frac{\rho}{M_p} \\
&& \kappa &= \frac{b_0}{2} + \frac{h_m}{\mu_{rec}}
\end{aligned}$$

$$\begin{aligned}
\phi(x_1) &= \beth \frac{\Gamma(x_1) \coth^2 \left[\frac{\pi}{\tau}(x_1 + h_m) \right]}{K_c^2(x_1)} \\
\psi(x_1) &= \frac{\nu\Gamma(x_1)B_{pmy}(x_1)}{K_c(x_1)} \coth \left[\frac{\pi}{\tau}(x_1 + h_m) \right] \\
\gamma(x_1) &= \frac{\beth}{K_c(x_1) \sinh \left[\frac{\pi}{\tau}(x_1 + h_m) \right]} \left[\eta - \frac{\zeta}{x_1 + \kappa} \right] \\
\tilde{\chi}(x_1) &= \chi\Gamma(x_1)B_{pmy}^2(x_1)
\end{aligned}$$

and defining $u_1 = i_{q1}$, $u_2 = i_{q2}$, $u_3 = i_{d1}$, $u_4 = i_{d2}$, those equations are described in a more compact form by

$$\begin{aligned}
 \dot{x}_1 &= x_2 \\
 \dot{x}_2 &= G - \phi(x_1)[2u_1^2 + u_2^2 + 2u_3^2 + u_4^2] - \tilde{\chi}(x_1) - \psi(x_1)[2u_3 + u_4] \\
 \dot{x}_3 &= x_4 \\
 \dot{x}_4 &= \gamma(x_1)u_2 \\
 \dot{x}_5 &= x_6 \\
 \dot{x}_6 &= 2\gamma(x_1)u_1.
 \end{aligned} \tag{39}$$

The values of the constants used in simulation are

μ_0	$4\pi \times 10^{-7}$	p_m	4
τ	0.0571	L_A	0.0500
τ_p	0.0286	B_r	1.0505
H_c	836000	μ_r	1.1000
h_m	0.0020	p	2

Table 1: Parameters of the motor considered for numerical calculations

4 Linear Control Design

Consider the problem of moving the platen to a desired set point in the space, i.e. $\mathbf{x}^d = [\bar{g}, 0, \bar{x}, 0, \bar{z}, 0]$. For the problem to be well-posed, one has to determine whether there exists a value of the control input $\mathbf{u} = [u_1, \dots, u_4]^T = \mathbf{u}^d$ that renders \mathbf{x}^d an equilibrium condition. For the previously specified constants, one finds that the problem is well-posed whenever \bar{g} is restricted within the range $0.035 \leq \bar{g} \leq 0.105$.

We designed an LQR controller based on the linearization of (39) around the equilibrium condition $(\mathbf{x}^d, \mathbf{u}^d)$ with

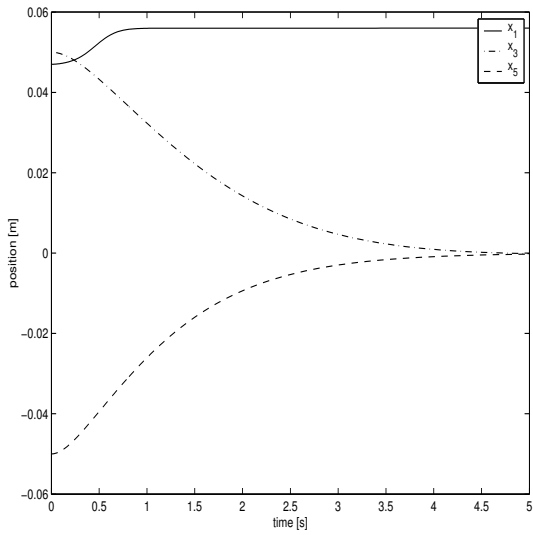


Figure 10: Position of the platen under LQR control for $x_1^d = 0.055m$ and $x_1(0) = 0.047m$

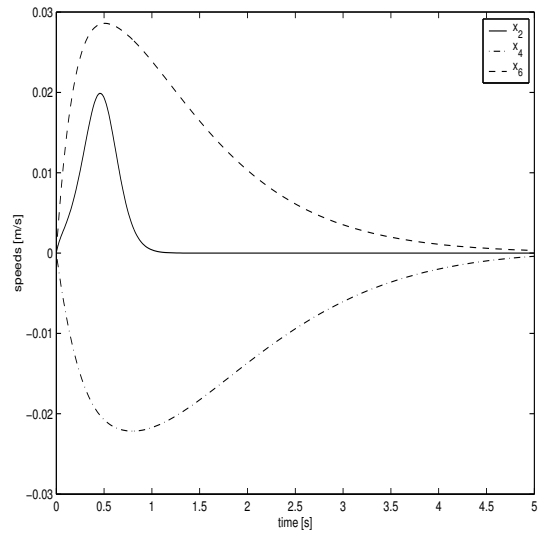


Figure 11: Speed of the platen under LQR control for $x_1^d = 0.055m$ and $x_1(0) = 0.047m$

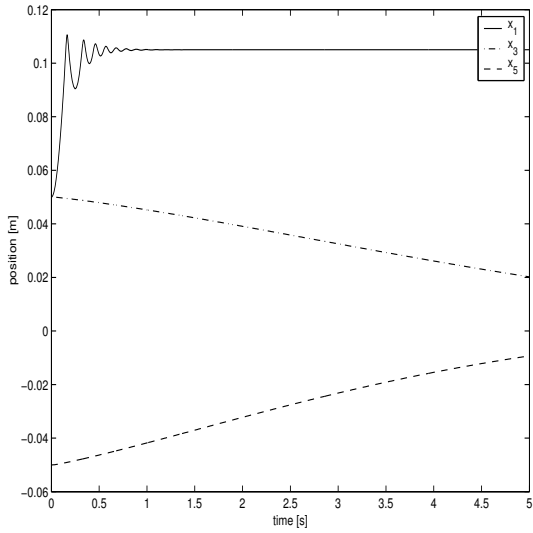


Figure 12: Position of the platen under LQR control for $x_1^d = 0.105m$ and $x_1(0) = 0.05m$

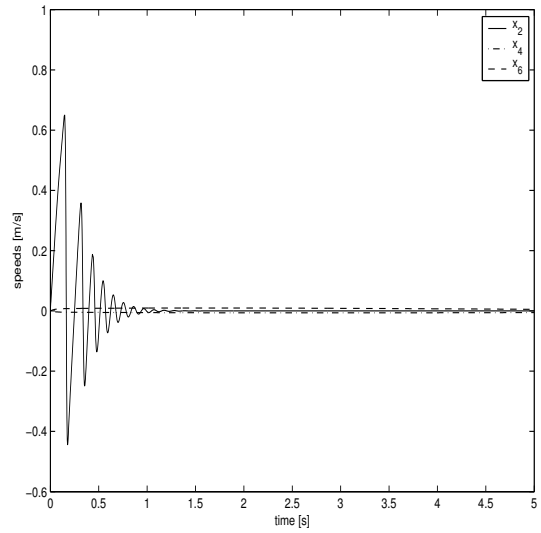


Figure 13: Speed of the platen under LQR control for $x_1^d = 0.105m$ and $x_1(0) = 0.05m$

the weighting matrices $Q = \text{diag}(100, 1, 1, 1, 1, 1)$ and $R = I_4$. The resulting feedback gain matrix is

$$K = \begin{bmatrix} 8.9173 & 0.7408 & 0.0000 & 0.0000 & 0 & 0 \\ 0 & 0 & 0 & 0 & 1.0000 & 1.3714 \\ -27.9235 & -2.3198 & -0.0000 & -0.0000 & 0 & 0 \\ -0.0000 & 0.0000 & 1.0000 & 1.6617 & 0 & 0 \end{bmatrix}. \quad (40)$$

Simulation results are shown in Figures 10 and 11, where the desired set point is $\mathbf{x}^d = [0.06, 0, 0, 0, 0, 0]^T$ and the initial condition is $\mathbf{x}(0) = [0.047, 0, 0.05, 0, -0.05, 0]^T$. The equilibrium inputs are $\mathbf{u} = [0, 0, -0.5, 1.1803]$.

Figures 12 and 13 show the simulation results with the equilibrium point set to $\mathbf{x}^d = [0.105, 0, 0, 0, 0, 0]^T$, $\mathbf{u}^d = [0, 0, -0.5, -0.7178]$, and the initial conditions set to $\mathbf{x}(0) = [0.05, 0, 0.05, 0, -0.05, 0]^T$.

5 Conclusions

The positioning device here proposed demonstrated to be linearly controllable within certain subset of the state space. Hence, smooth nonlinear control stabilization can be performed for this system. A rigorous nonlinear control law, developed on [9], has produced improved results as compared to the linear controller. Currently, a robust controller is being explored. Experimental implementation is under way.

References

- [1] S.A Nasar and G. Xiong, "Analysis of fields and forces in a permanent magnet linear synchronous machine based on the concept of magnetic charge," in *IEEE Transactions on Magnetics*, vol. 25, no. 3, May 1989.
- [2] S.A Nasar and G. Xiong, "Determination of the field of a permanent-magnet disk machine using the concept of magnetic charge," in *IEEE Transactions on Magnetics*, vol. 24, no. 3, May 1988.
- [3] I. Boldea and S.A. Nasar, *Linear electric actuators and generators*, Cambridge University Press, UK, 1997.
- [4] Z.Q. Zhu and D. Howe, "Instantaneous magnetic field distribution in brushless permanent magnet DC motors, part III: effect of stator slotting," in *IEEE Transactions on Magnetics*, vol. 29, no. 1, Jan 1993.

- [5] J.F. Gieras and Z.J. Piech, *Linear synchronous motors*, CRC Press LLC, USA, 2000.
- [6] W. Kim and D.L. Trumper, "High-precision levitation stage for photolithography", in *Precision Engineering* vol. 22, 1998, USA 1998
- [7] E. Weber, *Electromagnetic Theory: Static fields and their mapping*, Dover Publications, USA, 1965
- [8] J.F. Gieras and M. Wing, *Permanent Magnet Motor Technology, Design and Applications*, 2nd edition, Marcel Dekker Inc, USA, 2002
- [9] R. Becerril-Arreola, M. Maggiore, "Nonlinear Stabilization of a 3 degrees-of-freedom Magnetic Levitation System," accepted for publication at the American Control Conference 2003.